PHYSICAL REVIEW B **82**, 125315 (2010)

Stabilization of semiconductor surface reconstructions by configurational entropy

O. Romanyuk,[1,*] F. Grosse,[2] A. Proessdorf,[2] W. Braun,[2] and H. Riechert[2]
[1]*Institute of Physics, Academy of Sciences of the Czech Republic, Cukrovarnická 10, 162 00 Prague, Czech Republic*
[2]*Paul-Drude-Institut für Festkörperelektronik, Hausvogteiplatz 5-7, D-10117 Berlin, Germany*
(Received 17 August 2010; published 14 September 2010)

Surface unit cells with a larger area and a reduced symmetry have a larger configurational entropy. The entropy may even stabilize reconstructions with higher energy at finite temperatures. We study the entropy contribution to surface reconstructions on the basis of ground-state calculations employing density-functional theory. Specifically, the ground-state GaSb(111)*A* surface reconstruction has a (2×2) symmetry, but at elevated temperatures, we experimentally observe the $(2\sqrt{3}\times2\sqrt{3})$-$R30°$ symmetry in agreement with the theoretical results. The findings based on the general expressions are consistent with experimental data from other semiconductor surfaces.

DOI: 10.1103/PhysRevB.82.125315 PACS number(s): 68.35.B−, 68.35.Md, 68.47.Fg, 71.15.Mb

A theoretical prediction of the atomistic structure is important in different fields of science and technology. *Ab initio* calculations within density-functional theory (DFT) enable the prediction of structure and physical properties in the ground state, i.e., the state with lowest energy at zero temperature. At elevated temperature, however, entropic contributions can force a system into a state with higher energy.[1,2] Particularly, reconstructed crystal surfaces often exhibit small energy differences between alternative configurations which can be overcome by vibrational or configurational entropic contributions at typical preparation temperatures. For instance, entropic contributions have been found to play a role in the stabilization of metal surfaces,[3,4] oxide layers on metals,[5] as well as semiconductor surfaces[6,7] at elevated temperatures. Reconstructions on polar ZnO(001) surfaces[8] were found to be stabilized by vibrational entropy. On the other hand, the vibrational entropic contribution was estimated to be small for other systems.[9] The configurational entropy, focus of the present paper, is usually neglected. A general understanding of entropy-driven surface structure stabilization is therefore still lacking.

The thermodynamically stable surfaces of III-V semiconductors share common substructures or motifs such as homo- or heterodimers, trimers, and atomic vacancies, from which the reconstructions are assembled. The rearrangement of local motifs including changes in stoichiometry and unit-cell shape[10] is important to understand the experimentally observed diffraction pattern. In particular, certain Bragg reflections may vanish due to one-dimensional disorder, such as in the GaSb(001) (4×3) and GaAs(001) (2×4) reconstructions.[11–13] On the other hand, changes in the unit-cell translation periodicity, implying variations in the unit-cell size, are reflected by the number of fractional-order reflections along symmetrical azimuths in the diffraction pattern.

In the present work, the specific role of the size of the surface unit cell with respect to its configurational entropy contribution is analyzed. Based on the atomistic structure of the GaSb(111)*A* surface, we demonstrate theoretically how the surface changes its translation symmetry from the ground state (2×2) to the $(2\sqrt{3}\times2\sqrt{3})$-$R30°$ $(2\sqrt{3})$ symmetry at elevated temperatures. The theoretical prediction is confirmed experimentally under Sb-rich conditions and temperatures typical for molecular-beam epitaxy (MBE).

Total-energy *ab initio* calculations have been carried out for various GaSb(111)*A* (2×2) and $2\sqrt{3}$ phases. The vacancy buckling model [Fig. 1(a)] and top site trimer model [Fig. 1(b)] were suggested for different III-V(111)*A* semiconductor surfaces based on x-ray diffraction measurements,[14] photoemission measurements,[15] as well as DFT calculations.[16,17] The trimer model was proposed to exist under V-rich experimental conditions.[16] The considered III-V surface structures obey the electron counting rule[18] (ECR), i.e., the group III dangling bonds are empty and the group V dangling bonds are filled on a surface. The ECR is used as a guideline to build structure models with different III/V stoichiometries.

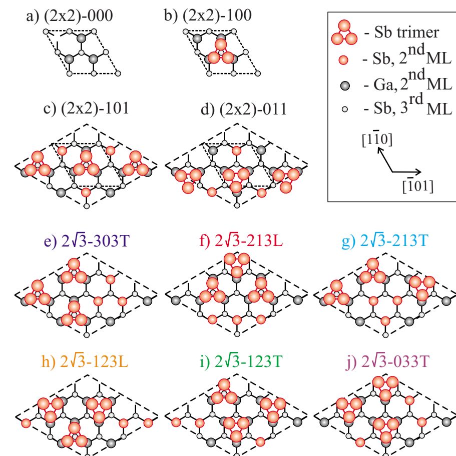

FIG. 1. (Color online) The GaSb(111)*A* [(a)–(d)] (2×2) and [(e)–(j)] $2\sqrt{3}$ structure models. The model notation $M-ijkT(L)$ refers to the translation periodicity M for (2×2) or $2\sqrt{3}$ unit cells. The number of Sb top (hollow) trimers within the unit cell is i (j). The number of Sb atoms in the second atomic layer is given by k. T (triangle) or L (line) optionally denote the local Sb atomic arrangements in the second atomic layer. (2×2) and $2\sqrt{3}$ unit cells are marked by a dashed rhombus. The Sb trimer can occupy (c) the top or (d) the hollow site. (c)–(j) cover all possible nonequivalent configurations within the Sb-rich stoichiometry for (2×2) and $2\sqrt{3}$ unit cells.

 ©2010 The American Physical Society

The calculations are carried out using the ABINIT computer code.[19,20] The local-density approximation for the exchange-correlation energy functional is applied. Norm-conserving pseudopotentials[21] of the Troullier-Martins type[22] are used to describe the atomic species. The electronic wave functions are expanded in a plane wave basis with a converged kinetic energy cutoff of 12 Ha and a **k** point set corresponding to 4×4 points per $2\sqrt{3}$ surface Brillouin zone.[23] The surface structures are constructed using the repeated supercell approach with a GaSb slab thickness of nine atomic layers, using equilibrium lattice parameters computed for bulk GaSb. A vacuum gap thickness of 15 Å is used. The bottom Sb layer of the slab is passivated by pseudohydrogens with 0.75 electronic charges. Atomic coordinates are adjusted until the interatomic forces become smaller than 10^{-4} Ha/Bohr, whereby only the three bottom layers (Ga-Sb-pseudo-H) are kept fixed. The $2\sqrt{3}$ unit-cell size is used in all calculations in order to use equivalent **k** point meshes. The surface energy density $\Delta\gamma$ is computed by the standard approach[16]

$$\Delta\gamma A = E_{tot} - (n_{\mathrm{Sb}} - n_{\mathrm{Ga}})\Delta\mu_{\mathrm{Sb}} - n_{\mathrm{Sb}}\mu_{\mathrm{GaSb}}^{bulk}, \quad (1)$$

where E_{tot} is the total energy of the system, μ_i the chemical potential of species i, n_i the number of atoms, and A the unit-cell area, respectively. The Ga-rich and Sb-rich experimental conditions correspond to the chemical potential range $-1<\Delta\mu_{\mathrm{Sb}}/H_f<0$, where $H_f=\mu_{\mathrm{Ga}}^{bulk}+\mu_{\mathrm{Sb}}^{bulk}-\mu_{\mathrm{GaSb}}^{bulk}=0.297$ eV is the heat of formation and $\Delta\mu_{\mathrm{Sb}}=\mu_{\mathrm{Sb}}-\mu_{\mathrm{Sb}}^{bulk}$.

We consider GaSb(111)A (2×2) and $2\sqrt{3}$ structure models across the full range from Ga-rich to Sb-rich compositions. The number of Sb trimers i located on top of Ga atoms and the number of Ga vacancies v are varied within the $2\sqrt{3}$ unit cell to cover all possible Ga/Sb stoichiometries. Additionally, we consider structure models where the Ga site in the second layer of the trimer model is substituted by an Sb atom [Fig. 1(c)]. The number of Sb atoms in the second atomic layer k is changed together with other motifs. This does not affect the fulfillment of the ECR since the charge produced by one Ga dangling bond (3/4 electrons) equals the charge produced by three Sb-Sb bonds and one Sb dangling bond (3/2–3/4 electrons). Structures with an Sb adatom on top of a Ga layer are not taken into account because of their high surface energy for other III-V(111)A surfaces.[16] We have calculated the total energies of the following models with the (ivk) configurations: (030) [Ga-rich, vacancy model], (120), (033), (121), (210), (123), (212), (300), (303) [Sb-rich]. All structures obey the ECR and can be assembled in a straightforward manner from the given number of structural motifs arranged within the $2\sqrt{3}$ unit cell.

The GaSb(111)A (2×2) and Sb-rich $2\sqrt{3}$ structure models are collected in Fig. 1. We have calculated models with other stoichiometries but they have higher surface energies and are therefore not included in the figure.

Depending on the local arrangement of the structure motifs, it is possible to obtain either a $2\sqrt{3}$ or a (2×2) periodicity with the same stoichiometry. The surface unit-cell size therefore depends on the arrangement of the structural motifs. All possible $2\sqrt{3}$ configurations within the Sb-rich stoichiometry are collected in Figs. 1(e)–1(j).

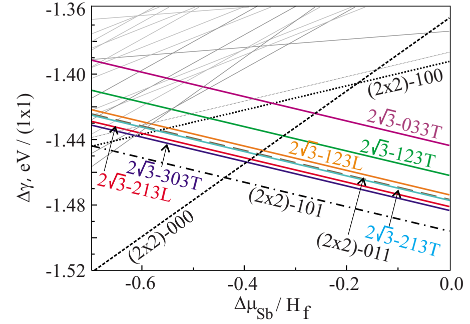

FIG. 2. (Color online) Surface formation energies for different GaSb(111)A structure models. Dashed and solid lines correspond to the (2×2) and $2\sqrt{3}$ reconstructions, respectively. The tilt of the lines reflects the Ga/Sb stoichiometry.

Figure 2 shows the surface formation energy diagram. The vacancy buckling model (2×2)-000 (Ga-rich) and the (2×2)-101 model (Sb-rich) are predicted to be thermodynamically stable. The Sb-rich $2\sqrt{3}$ structures are higher in energy by up to 52 meV/(1×1) for zero electronic temperature. The previously suggested trimer model (2×2)-100 (Refs. 16 and 17) is energetically unfavorable for GaSb(111)A. The hollow site trimer position is less favorable than the top site.

Although the zero temperature calculations predict the GaSb(111)A (2×2) structure to be stable, we experimentally observe a $2\sqrt{3}$ diffraction pattern. The surface is prepared on an on-axis, undoped GaSb(111)A substrate by MBE. The oxide is desorbed under a constant $\mathrm{Sb_4}$ flux of $\approx1\times10^{13}$ mol s^{-1} cm^{-2} at a substrate temperature of $T=470$ °C measured by a noncontact thermocouple. The sample is then cooled with 1°/s to $T=300$ °C. A buffer layer is grown at a rate of 0.05 ML/s with a constant III/V flux ratio of approximately 1:5 while the substrate temperature is ramped from 300 to 380 °C. The $\mathrm{Sb_4}$ overpressure on the surface is maintained during the measurement. The azimuthal scan in Fig. 3(a) is obtained by rotating the substrate around the surface normal while recording the intensity of the reflection high-energy electron-diffraction (RHEED) pattern.[24–26] During the measurement, the chamber pressure was 1×10^{-9} mbar and the electron beam energy was 20 keV.

Figure 3(a) shows the resulting azimuthal scan RHEED pattern of the GaSb(111)A surface under Sb-rich conditions[27] at $T=400$ °C. The $2\sqrt{3}$ symmetry is present. Nevertheless, the existence of (2×2) units cannot be ruled out since the corresponding peaks are common to both phases. The RHEED pattern measured at $T=400$ °C is given in Fig. 3(b). The electron beam runs along the $[\bar{2}11]$ azimuth. Fractional order rods lie on a 6× grid, where the rod at 3/6 [Fig. 3(b)] belongs to both the $2\sqrt{3}$ and (2×2) phases. Thus, this rod consists of scattering amplitudes from both (2×2) and $2\sqrt{3}$ domains, whereas other fractional order rods at 1/6, 2/6, 4/6, and 5/6 positions are due to $2\sqrt{3}$ scattering amplitudes only.

In Fig. 3(c), the integrated intensity ratios between the

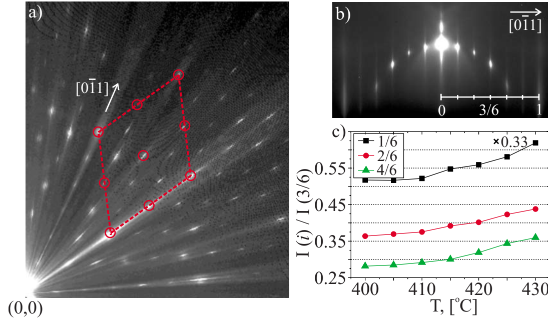

FIG. 3. (Color online) (a) Azimuthal scan RHEED diffraction pattern observed on a GaSb(111)*A* surface and (b) RHEED pattern measured along the [$\bar{2}$11] direction at T=400 °C. The (1×1) unit cell and the (2×2) diffraction spots are marked. The (2×2) and the $2\sqrt{3}$ diffraction patterns cannot be separated. (c) $2\sqrt{3}$ to (2×2) RHEED diffraction spot intensity ratios. The RHEED geometry presented in (b) is used for the measurements.

$2\sqrt{3}$ and the $2\sqrt{3}+(2\times2)$ fractional order reflections are shown. The sample is heated and cooled slowly with a rate of 0.05 °C/s under Sb-rich conditions. 12-bit RHEED images are acquired at 5 °C intervals. Integrated intensities around diffraction maxima and the background close by are measured. The background is subtracted. The intensity ratio changes with temperature. It confirms that the fraction of the $2\sqrt{3}$ phase increases with temperature at the expense of the (2×2) phase. The integrated intensities behave nearly identical during heating and cooling, showing negligible hysteresis. However, the given absolute value of the intensity ratio depends on the incidence beam angle as expected and can therefore be considered as a qualitative measure only.

Recently, InSb(111)*A* $2\sqrt{3}$ and (2×2) reconstructions were prepared by MBE.[28] A structure model with six Ga vacancies per surface unit cell was suggested based on scanning tunneling microscopy observations. Our DFT calculations do not confirm this model: the surface energy is at least 150 meV/(1×1) higher than for the (2×2)-101 reconstruction.

The vibrational entropy differences between the different structures can be ruled out as explanation since the unit cells differ only in the arrangement but not in the number of structure motifs. Therefore the next-nearest-neighbor configuration is identical for the reconstructions considered here. The vibrational properties will therefore be very similar, which leads to an approximately constant energy offset for all structures without affecting the configurational entropy.

Configurational entropy contributions at finite temperatures, however, can explain the stability of the higher energy $2\sqrt{3}$ structures. The concentration of a phase i in thermodynamical equilibrium at finite temperature is $c_i=Z_i/Z$, $i\in S$, where Z is the partition function and S covers all possible system states, i.e., phases. The partition function is expressed as follows:

$$Z=\sum_i Z_i=\sum_i g_i \exp\left(-\frac{\Delta\gamma_i A}{k_B T}\right), \tag{2}$$

where $\Delta\gamma_i$ is the surface energy of the ith phase with area A, k_B is the Boltzmann constant, and T is the temperature. The

TABLE I. Symmetry-determined degeneracy factor g_i, two-dimensional space-group number, number of symmetry operations σ_r, and energy differences $\Delta\Gamma=\Delta\gamma_{101}-\Delta\gamma_i$ [meV/(1×1)] relative to the energy of the (2×2)-101 structure for the different structure models. Model notations refer to notations in Fig. 1.

Model	No. (σ_r)	g_i	$\Delta\Gamma$	Model	No. (σ_r)	g_i	$\Delta\Gamma$
(c) (2×2)	14 (6)	4	0	(f) $2\sqrt{3}$	3 (2)	36	15
(d) (2×2)	14 (6)	4	19	(g) $2\sqrt{3}$	3 (2)	36	18
(e) $2\sqrt{3}$	15 (6)	12	12	(h) $2\sqrt{3}$	3 (2)	36	22
(j) $2\sqrt{3}$	15 (6)	12	52	(i) $2\sqrt{3}$	3 (2)	36	34

sum runs over all allowed symmetry inequivalent configurations within the considered cell (here $2\sqrt{3}$ cell).

The symmetry-dependent degeneracy factor g_i accounts for the number of symmetry equivalent structures. A general formula for g can be derived as follows. The underlying lattice for a crystalline surface is naturally given by (1×1) unit cells, defined by the projection of the bulk crystal structure onto the surface plane. A specific reconstruction covers a regular array of these unit cells, where the size of the two-dimensional Wigner-Seitz cell (reduced cell) in units of (1×1) cells is given by the product $n\times m$. Therefore, one can construct $n\times m$ equivalent reconstructions from each periodic surface configuration by simple translation. An additional contribution to g stems from the point symmetry of the surface unit cell which is less or equal than the symmetry of the (1×1) unit cell. Therefore, the total value of g_i is computed using the size of the unit cell $n_i\times m_i$ times a factor f_i, which is determined from the two-dimensional space-group symmetry of the unit cell,

$$g_i=f_i n_i m_i, \tag{3}$$

$$f_i=\sigma_{(1\times1)}/\sigma_r, \tag{4}$$

where $\sigma_{(1\times1)}$ and σ_r are the number of symmetry operations[29] for the ideal (1×1) and the reconstructed unit cells, respectively. For instance, an ideal GaSb(111) (1×1) surface would have the two-dimensional space-group number 14 ($p3m1$) and, consequently, the number of possible symmetry operations were $\sigma_{(1\times1)}=6$.

In Table I, g_i values are listed for the GaSb(111)*A* (2×2) and $2\sqrt{3}$ reconstructions. Unit cells with both top trimers and hollow sites (No. 3, $\sigma_r=2$, $n_i m_i=12$) have the lowest symmetry and the highest $g_i=36$. Phases terminated by trimers on top (or hollow) sites only have a higher surface symmetry (No. 15, $\sigma_r=6$) and, consequently, a smaller $g_i=12$. The smallest factors $g_i=4$ correspond to unit cells with the same number of symmetry operations but smaller cell size ($\sigma_r=6$, $n_i m_i=4$). A larger unit cell with lower surface symmetry is therefore more likely to exist on a given surface at elevated temperature.

The concentrations c_i of the reconstruction i is plotted in Fig. 4(a) as a funcion of the Sb chemical potential. The cumulated phase fractions of (2×2) and $2\sqrt{3}$ reconstructions are represented by black solid lines. Under Ga-rich conditions, only the (2×2)-000 structure is possible. The concen-

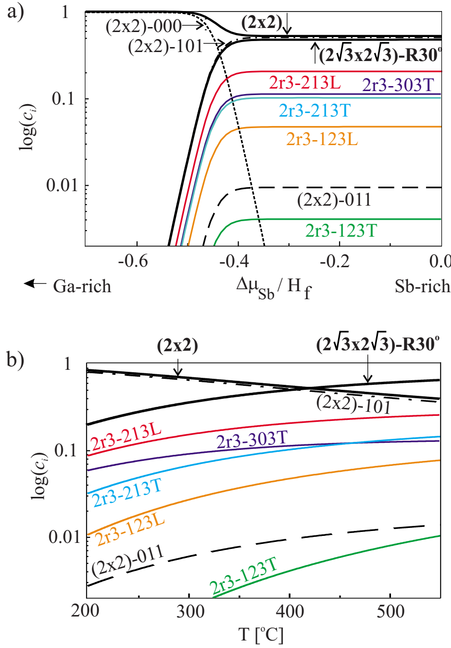

FIG. 4. (Color online) (a) Chemical potential and (b) temperature dependence of c_i at fixed chemical potentials $\Delta\mu_{\text{Sb}}/H_f=-0.3$. Phases with higher surface energies are also used in the calculation but not shown in the plot. The (2×2) and $2\sqrt{3}$ reconstructions coexist at finite temperature. Thick black solid lines represent the total concentrations of (2×2) and $(2\sqrt{3}\times2\sqrt{3})$-$R30°$ phases.

tration of this phase drops dramatically for $\Delta\mu_{\text{Sb}}/H_f>-0.5$ when Sb starts to adsorb on the surface. As a result, the probability of the $2\sqrt{3}$ phase increases.

The temperature dependence of the different phase fractions at a fixed chemical potential $\Delta\mu_{\text{Sb}}/H_f=-0.3$ is shown in Fig. 4(b). Such conditions can be achieved by adjusting the Sb flux together with the substrate temperature. The cumulated fraction of $2\sqrt{3}$ reconstructions is higher than the one of (2×2) units at $T>425$ °C. Thus, the entropic contribution increases the fraction of energetically less favorable phases at elevated temperature. This agrees with the $2\sqrt{3}$ to $2\sqrt{3}+(2\times2)$ RHEED intensity ratio measurements in Fig. 3(c), where the ratio changes with temperature. A high Sb flux is used during the RHEED measurements and the Sb chemical potential varies with temperature in the proximity of Sb-rich conditions. A fixed chemical potential such as in Fig. 4(b) is difficult to maintain in an experiment. Nevertheless, since the $2\sqrt{3}$ diffraction pattern does not disappear in the investigated temperature interval, the chemical-potential range can be estimated to lie in the interval $-0.3<\Delta\mu_{\text{Sb}}/H_f<0$. Therefore, the experiment confirms that the (2×2) phase concentration decreases with respect to the $2\sqrt{3}$ phase as predicted in Fig. 4(b).

When considering the energy of the reconstructed surface, we need to take into account that the boundary between two phases creates defects which raise the energy. In the case considered here, the unit cells differ only in the local arrangement of the motifs within the cells. The phase boundary energy is equal to the interaction energy between neighboring cells. For instance, the $2\sqrt{3}$-213L structure can be created from (2×2)-101 by moving one Sb atom and Sb trimer from a top to a hollow atomic site. By choosing one unit cell origin from the $2\sqrt{3}\times2\sqrt{3}=12$ possibilities, it is possible to match these unit cells without creating additional defects. The interaction energy is 3 meV/(1×1) in the case of combining (2×2)-101 and $2\sqrt{3}$-213L cells, which is close to the accuracy limit of our calculations. Thus, (2×2) and $2\sqrt{3}$ unit cells can coexist without additional domain boundary contributions at elevated temperatures.

Another example of local motif rearrangement is one-dimensional disorder due to low interaction energies between surface unit cells. Similar to the GaSb(001) (4×3) and GaAs(001) (2×4) reconstructions,[13] we have computed interaction energies for shifts between GaSb(111)*A* (2×2)-101 cells. A unit cell with a (2×2) size [Fig. 1(c)] is shifted by one surface lattice constant along the $[\bar{1}01]$ and $[1\bar{1}0]$ directions. The computed interaction energy is 2 meV/(1×1). This confirms the low interaction energy between structure motifs on the GaSb(111)*A* surface and, consequently, low energetic cost to increase the system's entropy.

To test the general validity of our approach, we have repeated the same calculations for the GaAs(111)*A* surface. On this surface, only the (2×2) pattern is experimentally observed.[30] This agrees with the computed larger energy differences between the (2×2) and $2\sqrt{3}$ phases that shift the transition to a $2\sqrt{3}$ pattern to a very high temperature. Furthermore, the various stoichiometries of the GaAs(001) $c(4\times4)$ structure[6] are a particular case of configurational entropic stabilization. In this case, structures with similar surface energies differ only in their two-dimensional space-group symmetries since all phases have the same unit-cell area. In general, however, the phase fraction depends on both the unit-cell area and the symmetry at nonzero temperature.

In summary, we have found and analyzed entropy-stabilized semiconductor surface reconstructions. *Ab initio* total-energy calculations carried out for the GaSb(111)*A* (2×2) and $2\sqrt{3}$ phases show that the (2×2)-101 structure has a lower surface energy than the previously suggested trimer model under Sb-rich experimental conditions. The GaSb(111)*A* $2\sqrt{3}$ Sb-rich phases have higher surface energies than the (2×2) phases. Nevertheless, the $2\sqrt{3}$ phases are stabilized by configurational entropy at elevated temperatures. A general form for the degeneracy factor g_i is proposed which explains the influence of the surface unit-cell size and the reduced symmetry on the entropy. Together with *ab initio* calculations, this formalism can be used for the surface structure analysis of crystalline materials at finite temperature.

Support by the German Research Foundation (bilateral Project No. 436 TSE 113/62/0-1), the Grant Agency of the Czech Republic (Grants No. P204/10/P028 and No. 20/07/0601), and by the Institutional Research Plan (Grant No. AV0Z 10100521) is gratefully acknowledged. Additionally, we would like to thank the project LUNA for additional computation capacity.

*romanyuk@fzu.cz

[1] B. J. Mhin, J. Kim, and K. S. Kim, Chem. Phys. Lett. **216**, 305 (1993).
[2] J. Kim, B. J. Mhin, S. J. Lee, and K. S. Kim, Chem. Phys. Lett. **219**, 243 (1994).
[3] P. Scharoch, Phys. Rev. B **80**, 125429 (2009).
[4] M. Borg, C. Stampfl, A. Mikkelsen, J. Gustafson, E. Lundgren, M. Scheffler, and J. N. Andersen, ChemPhysChem **6**, 1923 (2005).
[5] C. Stampfl, H. J. Kreuzer, S. H. Payne, H. Pfnür, and M. Scheffler, Phys. Rev. Lett. **83**, 2993 (1999).
[6] E. Penev, P. Kratzer, and M. Scheffler, Phys. Rev. Lett. **93**, 146102 (2004).
[7] J. C. Thomas, J. M. Millunchick, N. A. Modine, and A. Vander Ven, Phys. Rev. B **80**, 125315 (2009).
[8] M. Valtiner, M. Todorova, G. Grundmeier, and J. Neugebauer, Phys. Rev. Lett. **103**, 065502 (2009).
[9] K. Reuter and M. Scheffler, Phys. Rev. B **65**, 035406 (2001).
[10] O. Romanyuk, F. Grosse, and W. Braun, Phys. Rev. B **79**, 235330 (2009).
[11] O. Romanyuk, V. M. Kaganer, R. Shayduk, B. P. Tinkham, and W. Braun, Phys. Rev. B **77**, 235322 (2008).
[12] A. Ohtake, Surf. Sci. Rep. **63**, 295 (2008).
[13] O. Romanyuk, F. Grosse, and W. Braun, Phys. Status Solidi C **7**, 330 (2010).
[14] R. Feidenhans'l, M. Nielsen, F. Grey, R. L. Johnson, and I. K. Robinson, Surf. Sci. **186**, 499 (1987).
[15] T. van Gemmeren and R. L. Johnson, J. Phys.: Condens. Matter **9**, 4603 (1997).
[16] N. Moll, A. Kley, E. Pehlke, and M. Scheffler, Phys. Rev. B **54**, 8844 (1996).
[17] E. Pehlke, N. Moll, A. Kley, and M. Scheffler, Appl. Phys. A: Mater. Sci. Process. **65**, 525 (1997).
[18] M. D. Pashley, Phys. Rev. B **40**, 10481 (1989).
[19] X. Gonze *et al.*, Comput. Mater. Sci. **25**, 478 (2002).
[20] X. Gonze *et al.*, Z. Kristallogr. **220**, 558 (2005).
[21] M. Fuchs and M. Scheffler, Comput. Phys. Commun. **119**, 67 (1999).
[22] N. Troullier and J. L. Martins, Phys. Rev. B **43**, 1993 (1991).
[23] H. J. Monkhorst and J. D. Pack, Phys. Rev. B **13**, 5188 (1976).
[24] W. Braun, H. Möller, and Y. H. Zhang, J. Vac. Sci. Technol. B **16**, 1507 (1998).
[25] O. Romanyuk, K. Kataoka, F. Matsui, K. Hattori, and H. Daimon, Czech. J. Phys. **56**, 267 (2006).
[26] T. Abukawa, T. Yamazaki, K. Yajima, and K. Yoshimura, Phys. Rev. Lett. **97**, 245502 (2006).
[27] A. Proessdorf, F. Grosse, W. Braun, F. Katmis, H. Riechert, and O. Romanyuk (unpublished).
[28] M. Nishizawa, T. Eguchi, T. Misima, J. Nakamura, and T. Osaka, Phys. Rev. B **57**, 6317 (1998).
[29] *International Tables for Crystallography*, edited by T. Hahn (Kluwer Academic Publishers, Dordrecht, 2002), Vol. A, 5th edition.
[30] D. A. Woolf, D. I. Westwood, and R. H. Williams, Appl. Phys. Lett. **62**, 1370 (1993).